Progress In Electromagnetics Research C, Vol. 131, 35–48, 2023

A Compact 3D Printed Mirror Folded Lens Antenna for 5G Applications

Bin Xu and Bing Zhang*

Abstract—A concept to minimize the volume of a classic bifocal elliptical lens antenna is proposed. By applying the image theory, a reflective ground plane is placed along the short axis of a bifocal elliptical lens. An antenna-on-chip (AoC), as the lens' feed source, is placed at the upper focus and packaged by the lens body. The AoC radiates toward the ground plane instead of the free space. The geometric optics (GO) ray tracing analysis shows that the optical path of the miniaturized monofocal integrated lens antenna (ILA) is equal to that of the classic bifocal ILAs, so the gain is almost unaffected on the basis of the lens' volume reduction. For the quantitative evaluation of the gain loss caused by feed occlusion, a set of analytical equations is given. To verify the design concept, a 26 GHz miniaturized self-packaged monofocal elliptical ILA is designed and fabricated by 3D printing technology. The ILA achieves a 26.5 dBi gain and a size reduction rate of 38% compared with the classic bifocal elliptical lens. Moreover, the ILA also functions as the package for the AoC's die. The proposed design concept can not only reduce the volume of the classic bifocal elliptical lens dramatically but also save the effort and cost to package the AoC's die in a highly integrated system, which is believed to have great potential to create large profit margins for the fifth-generation (5G) mobile network applications.

1. INTRODUCTION

With the development of fifth-generation (5G) technology, applying millimeter-wave (mmWave) technologies to wireless communications becomes popular due to the wide bandwidth, high data rate, and low latency. Because of the considerable atmospheric attenuation, high-gain antennas are used to improve the communication quality [1–7]. Various processes and materials have been reported to fabricate planar mmWave antennas. Low temperature cofired ceramic (LTCC) antennas [6, 7], printed circuit board (PCB) antennas [8], plate laminated waveguide antennas [9], and metamaterials antennas [10, 11] are typical examples. However, the large-scale power distribution network to feed the planar array introduces additional loss and increases the manufacturing complexity.

Integrated lens antenna (ILA), which is often used together with an antenna-on-chip (AoC) as the feed source, is an effective solution to achieve high-gain mmWave antenna without the need for large-scale power distribution networks [12–23]. However, the bulky volume of an ILA is not desirable in 5G communications. Methods have been reported to reduce ILA's size, which basically falls into four categories. Firstly, increasing the relative permittivity of the lens material is a straightforward way to reduce lens size [12, 21]. Nonetheless, high-ε_r material usually has large weight, exorbitantly high price, and considerable loss. Meanwhile, high-ε_r material would result in high reflection and narrowband that extra matching layers and post process are needed [12, 19]. The second method is to design a heteromorphic profile to ensure an iso-phase surface on the lens' aperture [24, 25]. In this case, the lens can keep low profile and small size by using low-ε_r material, but the complex structure is a challenge for fabrication by either molding or machining. The third is to adopt inhomogeneous materials to build

Received 7 February 2023, Accepted 10 March 2023, Scheduled 15 March 2023
* Corresponding author: Bing Zhang (bzhang0609@hotmail.com).
The authors are with the College of Electronics and Information Engineering, Sichuan University, Chengdu 610065, P. R. China.

the synthetic dielectric lens (SDL) [13, 18, 26]. The drawback of this technique also lies in the difficulty of fabrication. Finally, partial filling, taking the form of periodical air cavities of different sizes, seems a good solution which is easy to manufacture and can help to reduce the weight of the lens to certain extent [27–29]. However, the periodical air cavities occupy much space, which makes the lens' size bulky. In the above-mentioned methods, though the size and weight of the integrated lens antenna have been effectively controlled, extra packages are still needed to provide physical protection and environmental isolation for the AoC's die in a highly integrated mmWave system, which asks for extra effort and cost in the design and fabrication of the package module.

In this paper, we propose a miniaturized, self-packaged, and low-cost monofocal elliptical ILA to be integrated with an mmWave antenna-on-chip. To minimize the volume of a classic bifocal elliptical lens in Fig. 1(a), a reflective ground plane is placed on the short axis. Applying the image theory, the sources located at the upper and lower focal points have similar properties when a sufficiently large metal plane exists in the central axis of the ILA. Applying the ray tracing method, a feed source radiating toward the reflective ground plane at the upper focal of the ILA in Fig. 1(b) is equal to that in Fig. 1(a), while the volume of the lens is minimized. Since the AoC is embedded in the lens in Fig. 1(b), the proposed lens also has the function of the antenna-on-chip die's package. The self-packaged characteristic of the lens eliminates the effort in designing and fabricating the package module, which can create large profit margins for the 5G applications. The subsequent gain loss from the feed occultation is studied. A set of equations to qualitatively evaluate the gain loss is derived from the ray tracing method. To verify the design concept, a 26 GHz lens prototype is fabricated by dielectric 3D printing technology using nylon. A patch antenna is used as the feed source to mimic the mmWave AoC. Benefitting from the truncated volume and self-packaged characteristic of the lens and from the low cost and short turn-around time of the 3D printing technology, the proposed ILA is an attractive antenna candidate for the 5G applications and highly integrated mmWave system.

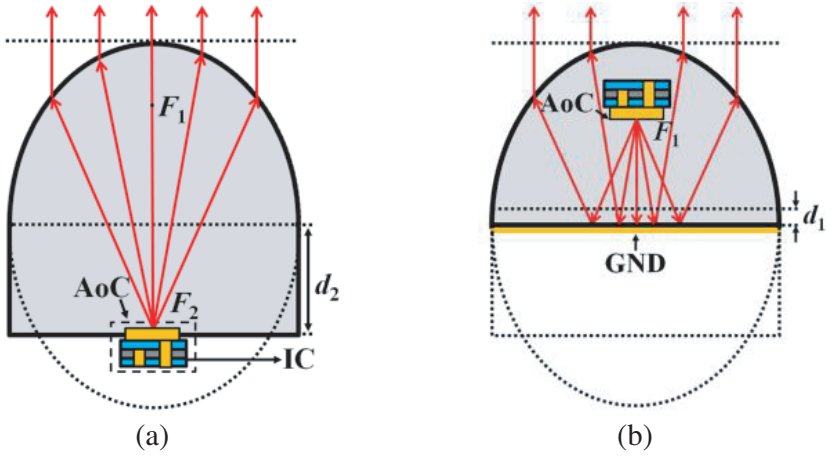

Figure 1. Comparison of the classic bifocal elliptical lens with the proposed ILA: (a) the classic bifocal elliptical lens and (b) the proposed ILA.

2. DESIGN AND ANALYSIS OF THE ILA

2.1. Design of the ILA

The geometry of the proposed ILA is shown in Fig. 2, and relevant parameters are listed in Table 1. It is composed of a monofocal elliptical lens, a feed source, and a reflective ground plane. As shown in Figs. 2(a) and (b), the proposed ILA has the same length of semi-long and short axis as the classic bifocal elliptical lens. The semi-long axis of the elliptical lens represents the half length of the long axis of the ellipse. The quarter-wave extension on the bottom is designed to reduce the influence of edge stray waves and to facilitate the fixation of the lens in practical applications. The sum of the height and quarter-wave extension of the proposed ILA is equal to the length of the semi-long axis of the classic

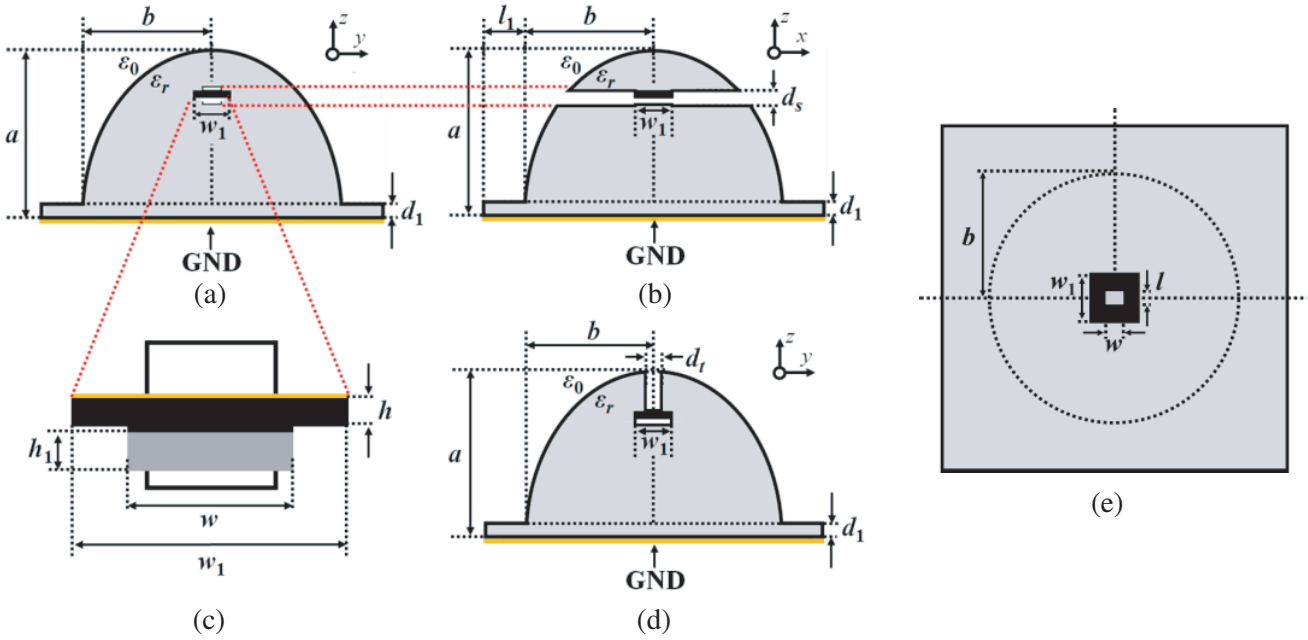

Figure 2. Geometry of the proposed ILA: (a) H-plane view of the side feeding ILA, (b) E-plane view of the side feeding ILA, (c) zoomed view of the patch and the air cavity, (d) H-plane view of the top feeding ILA, and (e) top view of the ILA.

Table 1. Geometric parameters of the ILA in Fig. 2 (Unit: mm).

Parameters	a	b	d_s	d_t
Value	75.88	60.22	2.4	2.4
Parameters	d_1	d_2	h	h_1
Value	3.12	49.23	0.508	1
Parameters	l	l_1	w	w_1
Value	3.37	23.26	4.6	12

bifocal elliptical lens. The metallic ground plays the role of reflecting electromagnetic waves from the feed source. Fig. 2(c) shows the zoomed view of the feed source, and the feed source radiates downward to the reflective ground plane in the proposed ILA. For ease of simulation and experiment, we use a patch antenna to mimic the AoC as the feed source in practical applications. An air cavity in the lens is designed to host the patch antenna. The space for the patch's feeding cable is also considered. Fig. 2(d) shows the top-feeding ILA of the same scale as Figs. 2(a) and (b), to evaluate the influence of the AoC's bias routing on the lens's performance. Fig. 2(e) shows the top view of the proposed ILA. The dashed curve outlines the lens's body. The solid curve outlines the lens's extension.

For an elliptical lens with relative permittivity ε_r, the refractive index n is expressed as $n = \sqrt{\varepsilon_r}$. The feed is placed at one of the focal points of the ellipsoid section to minimize the aberration of the lens and to obtain the desired focusing characteristics. The dimensions of the lenses are determined by the following relationship:

$$a = b\sqrt{\varepsilon_r/(\varepsilon_r - 1)} \tag{1}$$

$$d_2 = a/\sqrt{\varepsilon_r} \tag{2}$$

where a is the length of the semi-long axis of the elliptical lens which is also the height of the proposed lens; b is the length of the semiaxis of the elliptical lens which is also the waist radius of the proposed lens; and d_2 is the total combined cylindrical extension for the extended hemispherical approximation.

The eccentricity of the surface of a classic ILA is $e = 1/\sqrt{\varepsilon_r}$, and the gain is determined by the maximum waist radius b. We choose $b = 5.1\lambda_0$ to weigh the performance of the lens in this work.

2.2. Mechanism of Size Reduction

The ray tracing method based on geometrical optics (GO) is used to analyze the ILAs. The electromagnetic wave emitted from the feed is viewed as a ray, and each ray is traced to the field point separately. By analyzing and solving the electromagnetic field distribution radiated by the feed source, the electric field distribution on the aperture of the lens could be solved by integration.

As shown in Fig. 3(a), according to the ray tracing method, for the classical bifocal ILA to radiate plane waves, it needs to satisfy:

$$n\sqrt{x_N^2 + y_N^2} - y_N = n\sqrt{x_{N+1}^2 + y_{N+1}^2} - y_{N+1}, \quad N = 1, 2, 3 \ldots \tag{3}$$

where n is the refractive index of the lens. The surface electric field at the surface P_N can be calculated as shown in:

$$E_s = \hat{t} \cos^m \theta_s \cos\left(\frac{\pi}{h} z\right) e^{-jk|P_N F_2|} DF \cdot T_{\prod}(P_N), \quad N = 1, 2, 3 \ldots \tag{4}$$

where T_{Π} denotes the Fresnel parallel propagation coefficient at the point P_N; k denotes the propagation coefficient in the lens; z indicates the direction of propagation of electromagnetic waves; and DF denotes the diffusion factor on the surface of the elliptical lens, which is related to the ray incidence angle and refractive index.

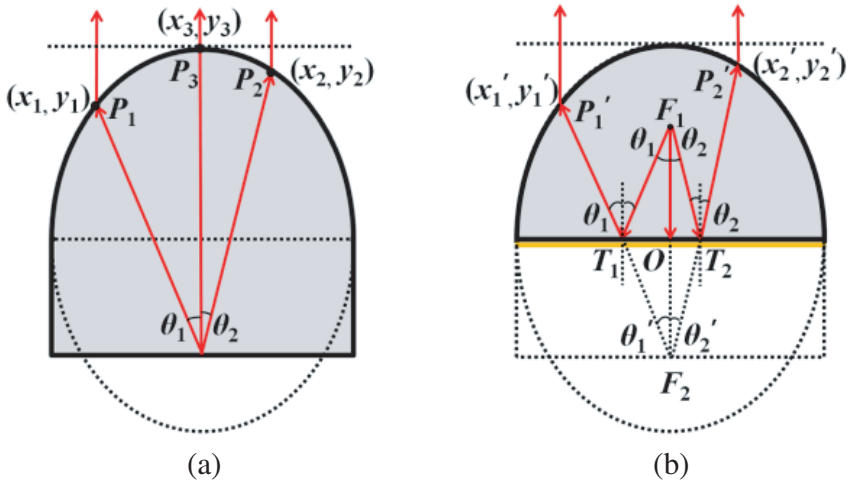

Figure 3. Lens models for ray tracing analysis: (a) the classic bifocal elliptical lens and (b) the proposed monofocal ILA.

The feed of the proposed monofocal self-packaged lens is located at the upper focal point. Through the boundary conditions and the image theory, the mirrored field source is located at the lower focal point of the ellipse, as shown in Fig. 3(b), i.e., $|OF_1| = |OF_2| = c$. By the law of reflection, the angle of incidence and reflection of each ray is the same as the angle of incidence of the mirrored source, i.e., $\theta'_N = \theta_N$, while $|F_1T_1| + |P'_1T_1| = |F_2P'_1|$. Each ray satisfies Eq. (3), and the propagation path is consistent with the classical bifocal ILAs. According to Eq. (4), the field magnitude at the outer surface of P'_N is the same as the field magnitude at P_N. Hence, the total gain of the lens does not change too much by mirroring the feed source.

When the optical path of the proposed ILA is analyzed by ray tracing, there are secondary or even higher reflected rays inside the lens. When the radius of the lens is much larger than the diameter of the feed source, the effect of multiple reflections can be neglected [30]. The electrical field distribution of a classic bifocal elliptical lens and the proposed ILA with identical conditions are given in Fig. 4. Figs. 4(a) and (b) show that both lenses radiate plane waves, and the electric field intensity is almost

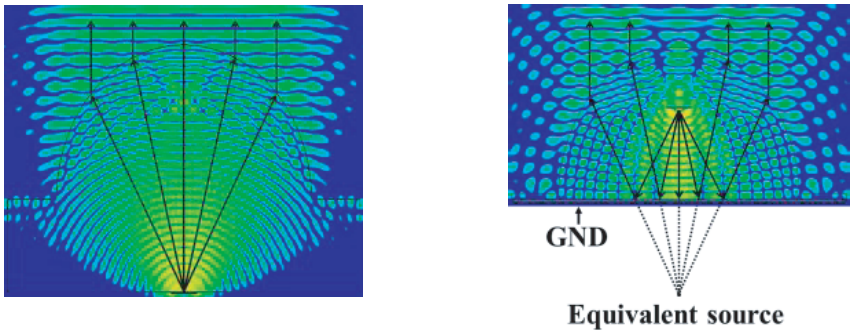

Figure 4. Electrical field distribution: (a) the classic bifocal elliptical lens in Figs. 3(a), and (b) the proposed monofocal ILA in Fig. 3(b).

the same. The field distributions in the space above the focal point are similar in Figs. 4(a) and (b), because the feed source is smaller than the lens, the EM coupling between the electromagnetic wave radiated from the feed source and the reflected wave is smaller in Fig. 4(b).

2.3. Design of the Feed Source

The proposed ILA packages the feed source inside the lens. The integrity of the feed source and lens should be considered systematically as a self-packaged antenna. To simplify the analysis, a microstrip patch antenna ($w = 4.6\,\text{mm}$ and $l = 3.37\,\text{mm}$) on Rogers RT5880 ($\varepsilon_r = 2.2$, $\tan\delta = 0.0009$) with substrate thickness $h = 0.508\,\text{mm}$ is used to mimic the AoC's die as the feed source. In order to host the patch antenna, leave space for the bias routing, and also reduce the impact of feeder matching to improve the performance of the ILA, an air cavity (AC) is designed inside the lens. The planar dimensions of the AC are the same as the patch antenna. The choice of the height of the AC h_1 is made considering three factors: 1) to leave enough space for the feed source and bias routing, 2) to alleviate the effect of dielectric loading, and 3) to ensure the phase perturbation caused by the AC will not influence the lens's aperture field distribution. In our design, we choose $h_1 = 1\,\text{mm}$ after optimization.

The performance of different lenses is shown in Fig. 5. The gain is reduced for the lens without AC. The reason is multiple reflections on the patch-lens interface. The dielectric loading is obvious when h_1 is smaller than 0.3 mm. As the height of the AC increases, the dielectric loading effect becomes

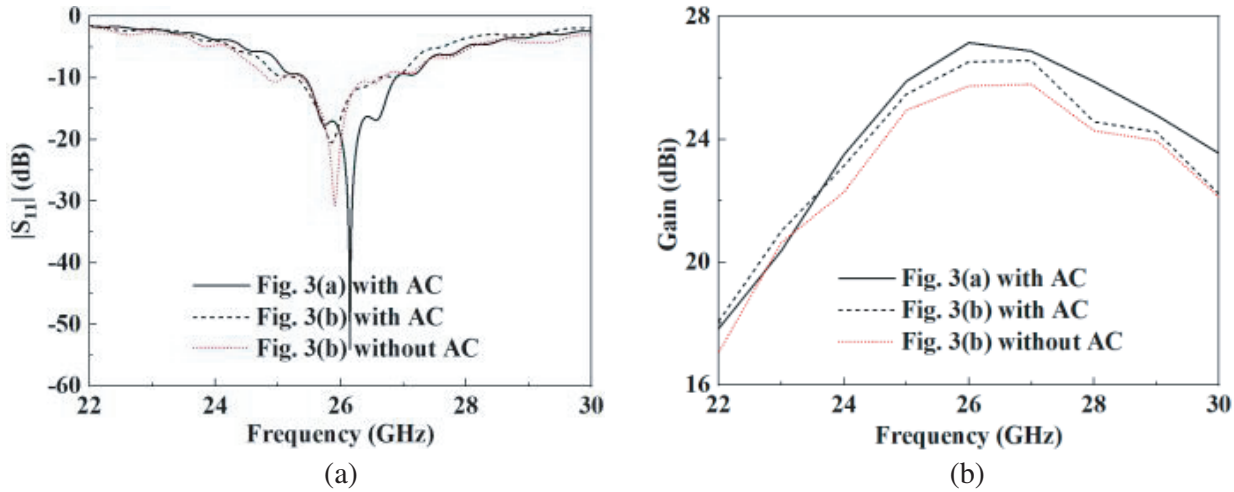

Figure 5. Performance of different lenses: (a) $|S_{11}|$ and (b) gain.

negligible. According to Fig. 5, the overall performances of the monofocal ILA in Fig. 3(a) and the bifocal lenses in Fig. 3(b) are almost the same after adding the AC. The maximum gain of 26.48 dBi appears at 26 GHz for the monofocal lens, while it is 27.15 dBi at 26 GHz for the bifocal lens. The gain difference is mainly caused by the feeding scheme.

2.4. Analysis of Radiation Characteristics of the ILA

The combination of the phase perturbation, the reflection, and the diffraction from the feeding cable would accumulate into a considerable disturbance of the lens' aperture field distribution, which possibly gives rise to decreased gain, tilted radiation pattern, and increased side lobe. The problem of feed occlusion can be studied with reference to that of the parabolic reflector. A quantitative evaluation of the feed occlusion of the ILA is informative for antenna designers.

2.4.1. Analysis of the Influence of the Feeding Cable

Since the patch antenna is packaged inside the lens, it is necessary to provide space for the feeding cable, which is denoted as d_s and d_t in Figs. 2(a) and (d), respectively.

For the side feeding ILA in Fig. 2(a), the slot for the feeding cable breaks the geometric symmetry of the lens. In the vicinity of the slot, power loss is caused by the inhomogeneity of the substrate, and the electromagnetic wave refracts on the interface between the slot and substrate of the lens according to Snell's law. Consequently, the wavefront of the lens is not an isophase plane, resulting in a gain decrement. With the increase of the feeding slot width d_s, the phase difference of the wave front becomes larger, and the gain of the ILA decrease. The ILA's gain versus slot size is given in Fig. 6. The gain is reduced by a total of 0.05 dB when d_s is varied from 0 mm to $\lambda_0/4$. The gain decreases by 0.3 dB when d_s is varied from 2.4 mm with a step of 2.4 mm. Fig. 7 shows the electric field distribution inside the lens. The feed cable is represented by a metallic cylinder, which is adjusted according to the size of the slot. In Figs. 7(a) and (b), the slot does not affect the formation of the planar wavefront. In Figs. 7(c) and (d), when the slot size exceeds $\lambda_0/4$, as the slot size increases, the phase difference between electromagnetic waves at different angles increases. The phase deviation of π diminishes the electric field at certain directions, which leads to an unequally distributed aperture field distribution and decreased gain. In this design, we choose $d_s = 2.4$ mm after optimization.

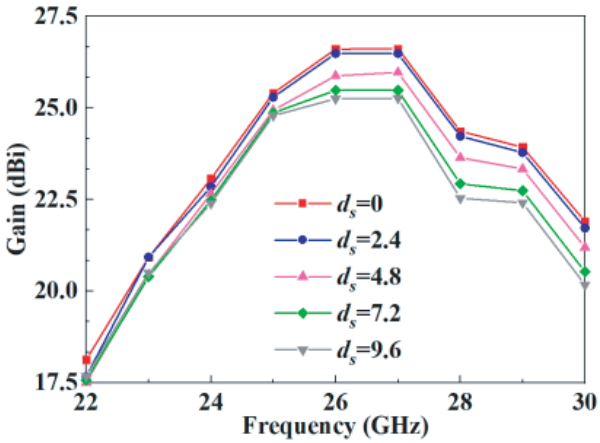

Figure 6. Gain of the side feeding ILA in Fig. 2(a) vs. the feeding slot width d_s.

A top-feeding ILA is designed for comparison, in which a large portion of the electromagnetic waves do not pass through the slot in the geometric axis of the lens with their phase unaffected. The wavefront remains an isophase plane, by which the radiation characteristics are almost unchanged. In general, as long as the feeding slot remains less than $\lambda_0/4$, the influence caused by the feeding slot on the ILA's performance is negligible.

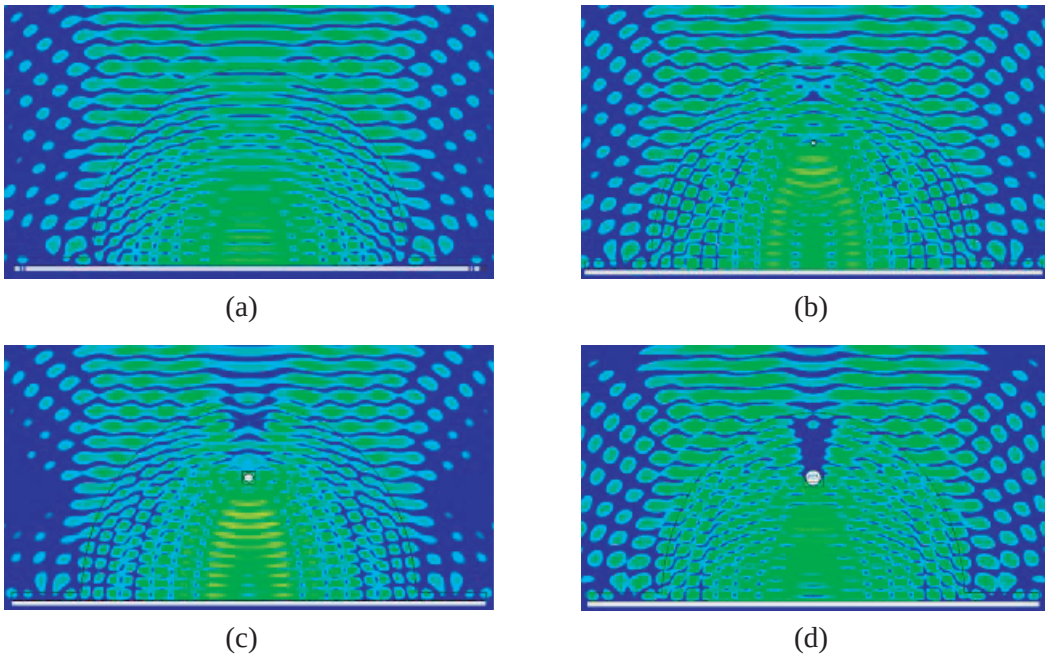

Figure 7. Electrical field distribution of the side feeding ILA in Fig. 2(a) on E-plane: (a) $d_s = 0\,\text{mm}$, (b) $d_s = 2.4\,\text{mm}$, (c) $d_s = 4.8\,\text{mm}$, and (d) $d_s = 7.2\,\text{mm}$.

2.4.2. Analysis of the Feed Occlusion

The feed occlusion refers to the impact of the antenna source on the radiation field of the main reflector or lens, which will affect the performance of the ILA. In the proposed ILA, a portion of the transmitted EM waves from the feed source is reflected by the ground plane back to the feed source, which causes the problem of feed occlusion and partial cancellation.

Figure 8 shows three different lenses for the feed occlusion study. For a fair comparison, b of the three lenses is the same as 60.22 mm. The gain difference ΔG_{A-B} between Lenses A and B is calculated by using the same feed source while the width of the metal dummy varies from 8 mm to 40 mm. The gain difference ΔG_{A-C} between Lenses A and C is calculated when the substrate width of the feed source

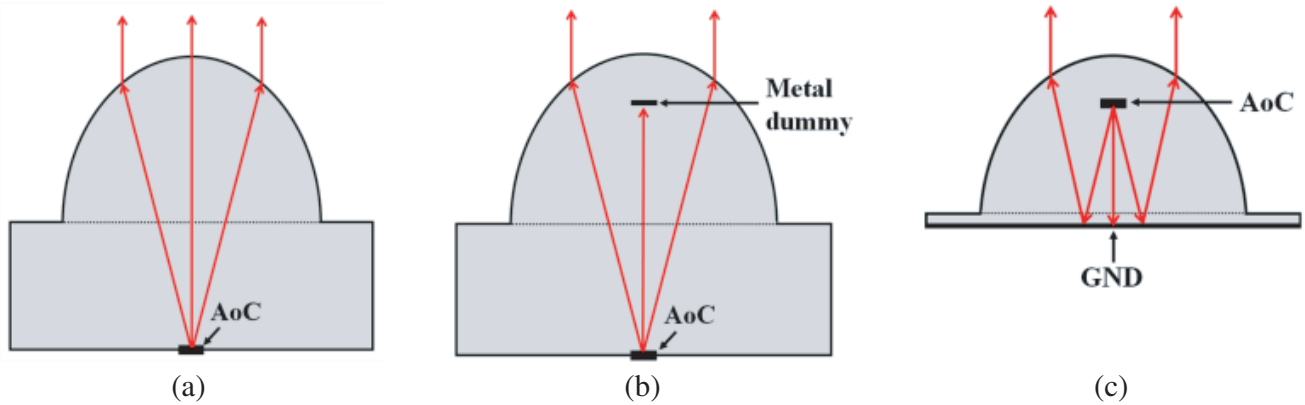

Figure 8. Three lenses for feed occlusion study: (a) Lens A: a classic bifocal elliptical lens with a feed source at the lower focal; (b) Lens B: a classic bifocal elliptical lens with a feed source at the lower focal and a metal dummy at the upper focal; (c) Lens C: the proposed monofocal ILA.

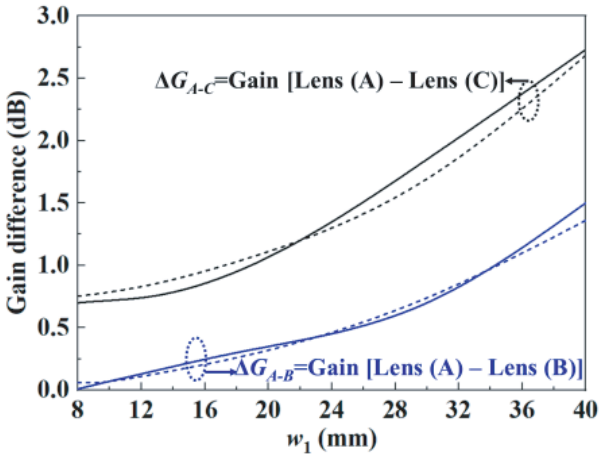

Figure 9. Gain difference vs. w_1 (w_1 indicates the substrate width and the metal dummy width in Fig. 8(b)): Simulated (solid line) and calculated (dotted line).

varies from 8 mm to 40 mm. As expected, the gain difference becomes larger as the feed occlusion becomes more obvious as shown in Fig. 9. It is quite straightforward to choose the minimum size of the feed source to avoid the gain decrement by feed occlusion. However, in a highly integrated mmWave system, a certain chip area should be left for the layout of other components such as mixers, amplifiers, filters, and sometimes even base band processors. A quantitative solution to evaluate the gain loss from the feed occlusion is important for system engineers to achieve a balanced design.

The gain difference ΔG_{A-B} between the two classic bifocal elliptical Lenses A and B can be calculated by

$$\Delta G_{A-B} = Gain\left[Lens\left(A\right) - Lens\left(B\right)\right] = -20\log\left(1 - \frac{w_1^2}{\pi b^2}\right) \tag{5}$$

in which w_1 is the width of the metal dummy in Fig. 8(b), and b is the waist radius of the lens. In Fig. 9, the simulated and calculated ΔG_{A-B} show good agreement, which proves the accuracy of Eq. (5).

The problem of feed occlusion in the proposed ILA is similar to that of an in-focal-fed parabolic reflector [31]. The problem of feed occlusion could also be analyzed using a similar quantification method. Fig. 10 shows the quantification of the radiation model of the feed source and monofocal ILA.

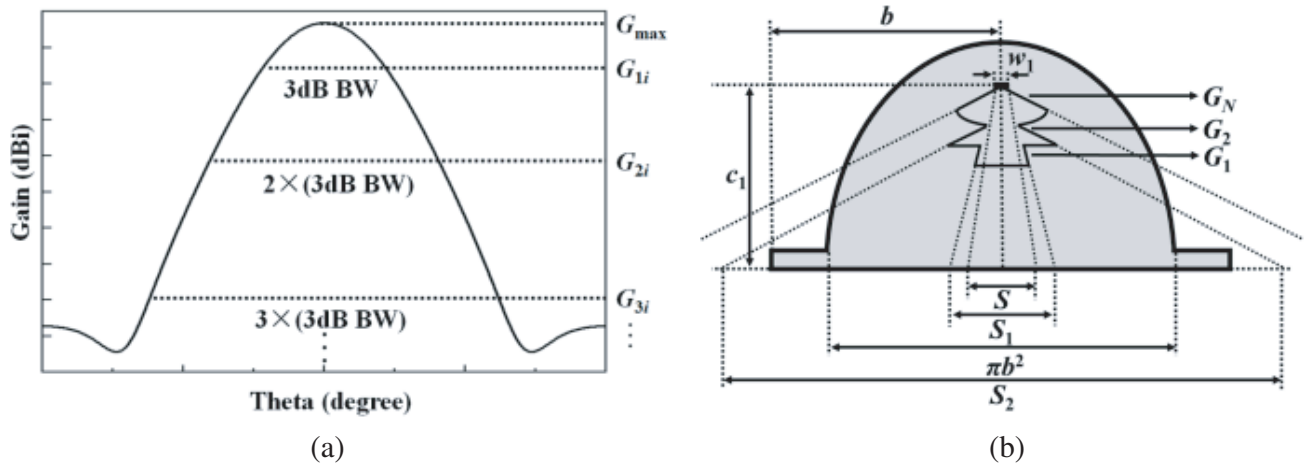

Figure 10. Quantification of the radiation model of the: (a) feed source and (b) proposed ILA.

The concept of feed source quantification is expressed as

$$G_1 = \frac{G_{\max} + G_{1i}}{2}, G_2 = \frac{G_{1i} + G_{2i}}{2}, \ldots, G_N = \frac{G_{(N-1)i} + G_{Ni}}{2}, \quad N = 1, 2, 3 \ldots \tag{6}$$

The E- and H-planes refer to the directional plane parallel to the direction of the electric field and the magnetic field, respectively. In case that the feed source has an asymmetric radiation pattern on E- and H-planes, the quantification could also be carried out as

$$G_{Ni} = 10^{(G_E + G_H)/20} \tag{7}$$

where G_E and G_H are the normalized gains on E- and H-planes, respectively. After normalizing $G_2 \ldots G_N$ against G_1 and setting G_1 as 1, the gain difference ΔG_{A-C} between Lenses A and C can be calculated as

$$S = \frac{c_1 w_1}{k_1} \tag{8}$$

$$\eta = \frac{G_1 \times (S_1 - S) + G_2 \times (\pi b^2 - S_1)}{G_1 \times S_1 + G_2 \times \pi b^2} \tag{9}$$

$$\Delta G_{A-C} = Gain\left[Lens\left(A\right) - Lens\left(C\right)\right] = 10 \log\left(\frac{1}{\eta}\right) \tag{10}$$

where η is feed occlusion factor, S_1 the projected area of gain G_1 on the ground plane confined by the feed source's 3 dB beamwidth, c_1 the half focal length, w_1 the substrate width of the feed source, k_1 an empirical factor of 35, $G_1 = 1$, and $G_2 = 0.327$ in our design. Simulated and calculated ΔG_{A-C} agree well in Fig. 9. It proves the accuracy of the proposed equations for quantitative analysis of the feed occlusion, which is important for system engineers to achieve a balanced design between the lens performance and system integrity. It is worth mentioning that if an active antenna is used as the feed source, which includes not only the antenna but also other active circuits and control modules, the footprint of the feed source might increase, which leads to increased feed occlusion. This can be solved by using hybrid processes to fabricate the active antenna, which stacks up circuits vertically. Thus, the footprint of the feed source might not be increased. To dissipate the heat generated by the active feed source, air holes could be drilled to facilitate the airflow for heat dissipation.

3. FABRICATION AND MEASUREMENT

To verify the design concept, two ILA prototypes in Figs. 2(a) and (d) are fabricated. Fig. 11 shows photographs of ILAs which are fabricated by stereolithography apparatus (SLA) technology using white nylon PA12 ($\varepsilon_r = 2.6$, $\tan\delta = 0.005$) and the antenna measurement setup. For the feed source placement, the ILA is divided into upper and lower parts. The bottom of the lower part is covered by copper foils that function as the reflective ground plane. In addition, a lens top cover for the top-feeding (top right corner in Fig. 11) was also printed in order to explore the influence of the feeder and solder sections in practical applications. The performance of the antenna was simulated by CST 2019. It is worth mentioning that the performance of top feeding ILA is similar to the side feeding ILA in Figs. 12–14. For the page limit of the communication, the top feeding ILA's performance will not be introduced.

Figure 12 depicts simulated and measured $|S_{11}|$ of the ILA. There is a little frequency shift for the ILA, which is caused by the fabrication tolerance. The far-field performance of the proposed ILA is measured by an in-house antenna measurement setup. Fig. 13 shows the normalized radiation patterns of ILA at different frequencies. Figs. 13(a) and (b) show the normalized total gain at center frequency 26 GHz, and the simulated gain is 26.48 dBi, while it is 25.86 dBi in measurement. The difference is caused by the geometric asymmetry and feeder loss, which is closely related to the radiation of the feeder section. Figs. 13(c)–(f) show the normalized total gain of the ILA at 25 and 27 GHz. Radiation patterns of the lens are consistent throughout the bandwidth, and the cross-polarization is less than -20 dB. Parasitic radiations from the induced current on the RF feeding cable break the symmetry of the aperture field distribution of the lens, which gives rise to the increased side lobe and deteriorated cross-polarization level on the E-plane. In practical applications, the feeders are packaged with the

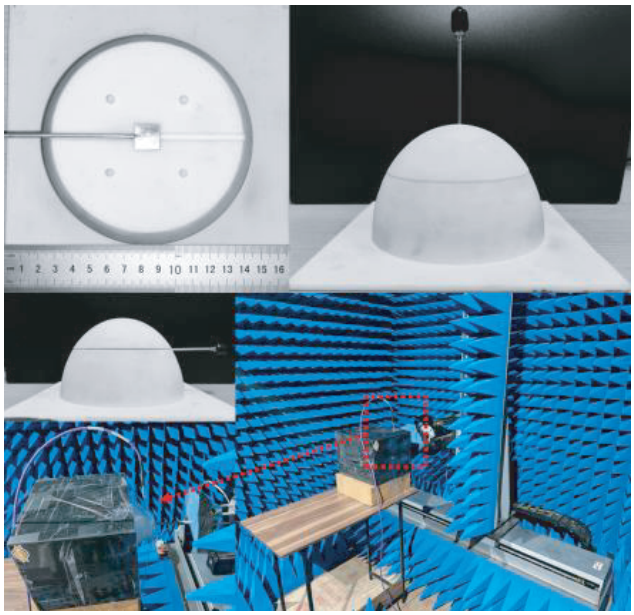

Figure 11. Photographs of the fabricated ILA and the measurement setup.

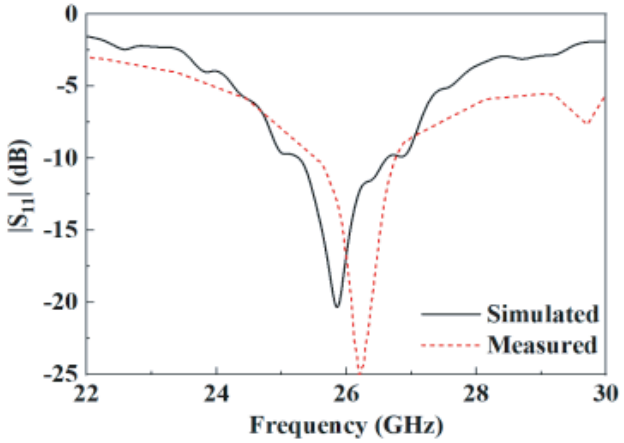

Figure 12. $|S_{11}|$ of the proposed ILA.

Table 2. Comparison between ILAs.

Ref.	[18]	[27]	[28]	This work
Freq. (GHz)	28	28	60	26
Size reduction ratio	48%	13%	12%	38%
Height/Diameter	54%	92%	86%	61.3%
Gain (dBi)	10	19	21.4	26.5
Aperture efficiency	1.9%	77.3%	87.5%	42%
X-pol (dB)	-35	NA	-15	-25
Self-packaged	No	No	No	Yes

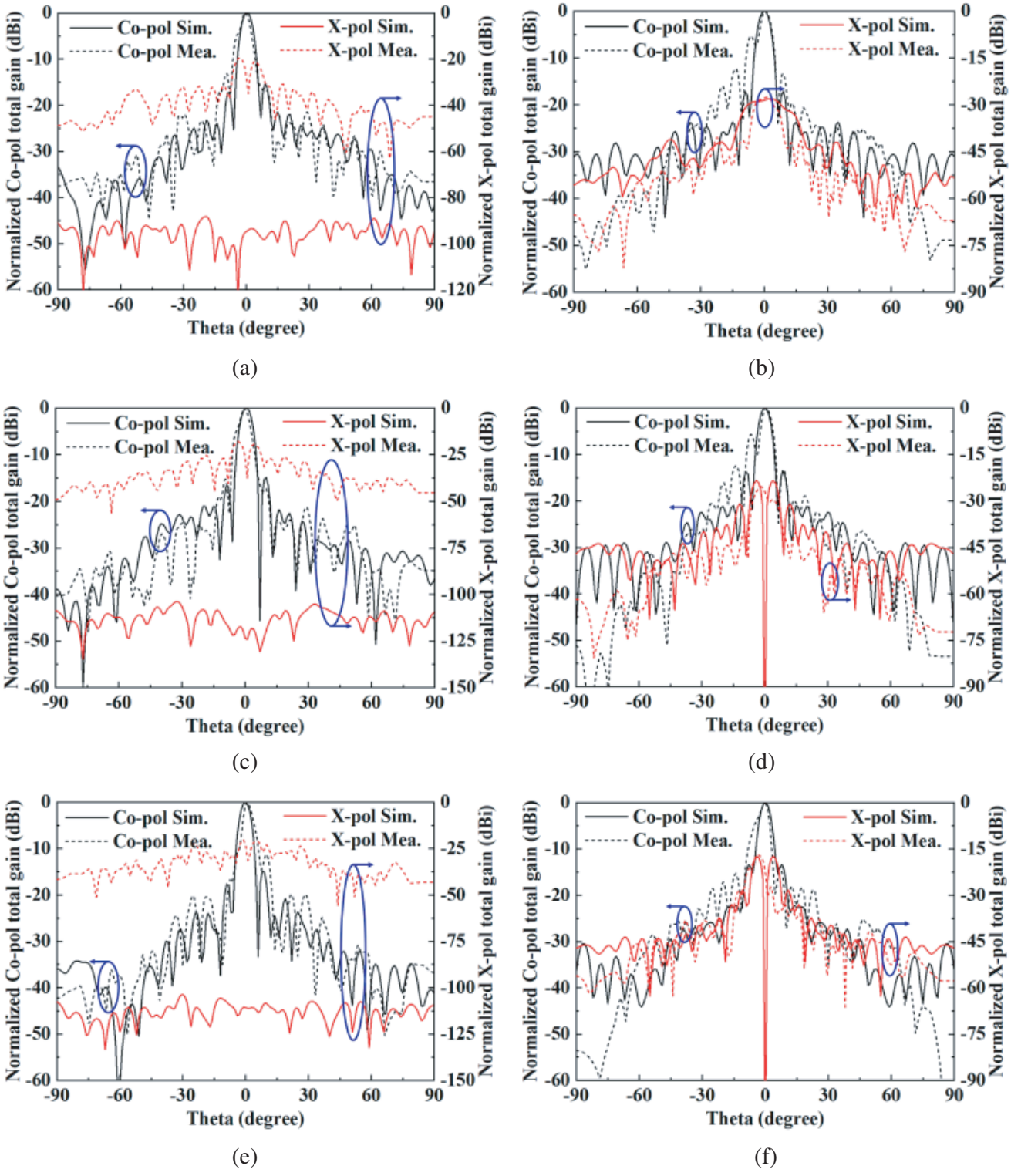

Figure 13. Normalized radiation patterns of the proposed ILA at different frequencies. 26 GHz: (a) E- and (b) H-planes; 25 GHz: (c) E- and (d) H-planes; 27 GHz: (e) E- and (f) H-planes.

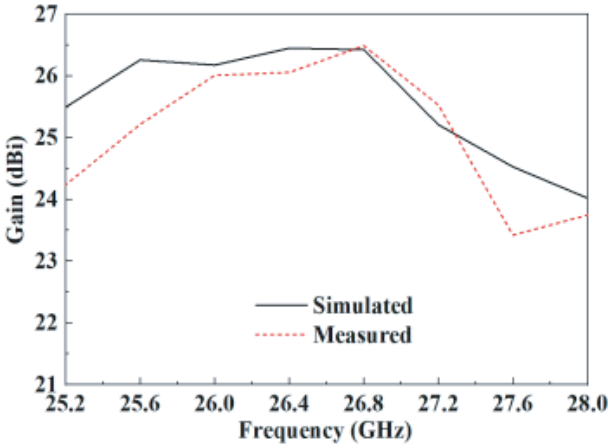

Figure 14. Simulated and measured gain.

circuit modules and produced by machine, which minimizes the impact of this part. Fig. 14 shows the gain curves in and around the bandwidth of the ILA. There is a little frequency shift that consistent with the $|S_{11}|$.

Table 2 compares the proposed ILA with other reported works. In [18], the lens has an irregular profile with a matching layer. Although the size reduction is satisfactory, the gain is greatly affected. Due to the irregular shape of the curved profile, it is not easy to manufacture. In [27] and [28], gains are much higher than that in [18]. However, those lenses have bulky size. The above-mentioned ILAs place a feed source outside the lens body. An extra package is needed for the feed source when it is going to be used in a highly integrated system. The proposed ILA in this work, taking the form of a simple elliptical profile, features the highest gain with desirable size reduction ratio and height/diameter ratio. The self-packaged characteristic of the proposed ILA eliminates the need to design and fabricate the chip package module. The use of 3D printing technology further reduces cost and turn-around time of fabrication. With the high gain, miniaturized profile, self-packaged characteristic, low cost, and moderate aperture efficiency, the proposed ILA is a preferable choice for 5G applications.

4. CONCLUSION

A miniaturized self-packaged ILA is proposed. According to the image theory, a classic bifocal elliptical lens is transformed into a monofocal elliptical lens by placing a reflective ground plane along its short axis, while the antenna gain is not much affected. An AoC, as the feed source, is placed at the upper focus of the ILA and radiates toward the reflective ground plane. Since AoC is embedded in the lens, the lens also functions as the package for the AoC's die. A set of equations is derived to quantitatively evaluate the gain loss from the feed occlusion. The 3D printing technology is used to fabricate the lens, which further reduces the fabrication cost and turn-around time. The proposed lens antenna features high gain, small size, self-packaged characteristic, and low cost. It is a capable antenna candidate for the 5G applications and has high potential in the satellite communication field, satellite earth exploration, and space research operations. The design concept and equations for feed occlusion evaluation provide a systematic thought for engineers.

ACKNOWLEDGMENT

This work is supported by the National Natural Science Foundation of China under grant 62171301, the State Key Laboratory of Millimeter Waves under grant K202322, and the State Key Laboratory of Polymer Materials Engineering under grant sklpme 2022-2-03.

REFERENCES

1. Ye, Q., Y. Zhang, and S. Zhang, "High-isolation dual-polarized leaky-wave antenna with fixed beam for full-duplex millimeter-wave applications," *IEEE Trans. Antennas Propag.*, Vol. 69, No. 11, 7202–7212, Nov. 2021.
2. Zhang, B., H. Zirath, and Y. P. Zhang, "Investigation on 3-D-printing technologies for millimeter-Wave and Terahertz applications," *Proc. IEEE*, Vol. 105, No. 4, 723–736, Apr. 2017.
3. Zhang, B., H. Sun, and K. Huang, "A metallic 3-D printed airborne high-power handling magneto-electric dipole array with cooling channels," *IEEE Trans. Antennas Propag.*, Vol. 67, No. 12, 7368–7378, Dec. 2019.
4. Nuaimi, M., W. Hong, and Y. Zhang, "Design of high-directivity compact-size conical horn lens antenna," *IEEE Antennas Wireless Propag. Lett.*, Vol. 13, 467–470, 2014.
5. Li, Y. and K. Luk, "Low-cost high-gain and broadband substrate- integrated waveguide fed patch antenna array for 60-GHz band," *IEEE Trans. Antennas Propag.*, Vol. 62, No. 11, 5531–5538, Nov. 2014.
6. Zhu, J., Y. Yang, and Q. Xue, "Low-profile wideband and high-gain LTCC patch antenna array for 60 GHz applications," *IEEE Trans. Antennas Propag.*, Vol. 68, No. 4, 3237–3242, Apr. 2020.
7. Zhu, J., C. Chu, and Q. Xue, "60-GHz high gain planar aperture antenna using Low-Temperature Cofired Ceramics (LTCC) technology," *IEEE MTT-S International Wireless Symposium (IWS)*, 1–3, 2019.
8. Wong, H., K. Luk, and H. Lai, "Small antennas in wireless communications," *Proc. IEEE*, Vol. 100, No. 7, 2109–2121, Jul. 2012.
9. Miura, Y., J. Hirokawa, and G. Yoshida, "Double-layer full-corporate-feed hollow-waveguide slot array antenna in the 60-GHz band," *IEEE Trans. Antennas Propag.*, Vol. 59, No. 8, 2844–2851, Aug. 2011.
10. Arfan, M. A. and H. Alqahtani, "Scattering of Laguerre-Gaussian beam from a chiral-coated perfect electromagnetic conductor (PEMC) cylinder," *Journal of Computational Electronics*, Vol. 21, No. 1, 253–262, 2022.
11. Arfan, M. and S. Rehman, "Laguerre-Gaussian beam scattering by a perfect electromagnetic conductor (PEMC) sphere," *Arabian Journal for Science and Engineering*, 2022.
12. Nguyen, N., N. Delhote, and R. Sauleau, "Design and characterization of 60-GHz integrated lens antennas fabricated through ceramic stereolithography," *IEEE Trans. Antennas Propag.*, Vol. 58, No. 8, 2757–2762, Aug. 2010.
13. Costa, J., C. Fernandes, and H. Legay, "Compact Ka-band lens antennas for LEO satellites," *IEEE Trans. Antennas Propag.*, Vol. 56, No. 5, 1251–1258, May 2008.
14. Bisognin, A., N. Nachabe, and C. Luxey, "Ball grid array module with integrated shaped lens for 5G backhaul/fronthaul communications in F-band," *IEEE Trans. Antennas Propag.*, Vol. 65, No. 12, 6380–6394, Dec. 2017.
15. Bisognin, A., D. Titz, and C. Luxey, "3D printed plastic 60 GHz lens: Enabling innovative millimeter wave antenna solution and system," *IEEE MTT-S International Microwave Symposium (IMS)*, 1–4, 2014.
16. Wu, X., G. Elefteriades, and T. Perkins, "Design and characterization of single- and multiple-beam mm-wave circularly polarized substrate lens antennas for wireless communications," *IEEE Trans. Microwave Theory Tech.*, Vol. 49, No. 3, 431–441, Mar. 2001.
17. Godi, G., R. Sauleau, and D. Thouroude, "Performance of reduced size substrate lens antennas for millimeter-wave communications," *IEEE Trans. Antennas Propag.*, Vol. 53, No. 4, 1278–1286, Apr. 2005.
18. Nguyen, N., R. Sauleau, and L. Coq, "Reduced-size double-shell lens antenna with flat-top radiation pattern for indoor communications at millimeter waves," *IEEE Trans. Antennas Propag.*, Vol. 59, No. 6, 2424–2429, Jun. 2011.

19. Nguyen, N., R. Sauleau, and C. Perez, "Very broadband extended hemispherical lenses: Role of matching layers for bandwidth enlargement," *IEEE Trans. Antennas Propag.*, Vol. 57, No. 7, 1907–1913, Jul. 2009.
20. Nguyen, N., R. Sauleau, and L. Coq, "Focal array fed dielectric lenses: An attractive solution for beam reconfiguration at millimeter waves," *IEEE Trans. Antennas Propag.*, Vol. 59, No. 6, 2152–2159, Jun. 2011.
21. Filipovic, D., S. Gearhart, and G. Rebeiz, "Double-slot antennas on extended hemispherical and elliptical silicon dielectric lenses," *IEEE Trans. Microwave Theory Tech.*, Vol. 41, No. 10, 1738–1749, Oct. 1993.
22. Fernandes, C., E. Lima, and J. Costa, "Broadband integrated lens for illuminating reflector antenna with constant aperture efficiency," *IEEE Trans. Antennas Propag.*, Vol. 58, No. 12, 3805–3813, Dec. 2010.
23. Fan, C., W. Yang, and Q. Xue, "A wideband and low-profile discrete dielectric lens using 3-D printing technology," *IEEE Trans. Antennas Propag.*, Vol. 66, No. 10, 5160–5169, Oct. 2018.
24. Bares, B. and R. Sauleau, "Electrically-small shaped integrated lens antennas: A study of feasibility in Q-band," *IEEE Trans. Antennas Propag.*, Vol. 55, No. 4, 1038–1044, Apr. 2007.
25. Rolland, A., M. Ettorre, and R. Sauleau, "Axisymmetric resonant lens antenna with improved directivity in Ka-band," *IEEE Antennas Wireless Propag. Lett.*, Vol. 10, 37–40, 2011.
26. Nguyen, N., R. Sauleau, and M. Ettorre, "Finite-difference time-domain simulations of the effects of air gaps in double-shell extended hemispherical lenses," *IET Microwaves, Antennas Propag.*, Vol. 4, No. 1, 35–42, Jan. 2010.
27. Nguyen, N., A. Rolland, and R. Sauleau, "Size and weight reduction of integrated lens antennas using a cylindrical air cavity," *IEEE Trans. Antennas Propag.*, Vol. 60, No. 12, 5993–5998, Dec. 2012.
28. Wang, K. and H. Wong, "Design of a wideband circularly polarized millimeter-wave antenna with an extended hemispherical lens," *IEEE Trans. Antennas Propag.*, Vol. 66, No. 8, 4303–4308, Aug. 2018.
29. PourMousavi, M., M. Wojnowski, and R. Weigel, "The impact of shape and size of air cavity on extended hemispherical lens characterization for wireless applications at 61 GHz," *Proc. Seventh Eur. Conf. Antennas and Propag. (EuCAP)*, 3295–3298, 2013.
30. Pavacic, A., D. Rio, and G. Eleftheriades, "Three-dimensional ray-tracing to model internal reflections in off-axis lens antennas," *IEEE Trans. Antennas Propag.*, Vol. 54, No. 2, 604–612, Feb. 2006.
31. Wang, J., Z. Wang, and H. Zhang, "Fast calculation of shading effect of reflector antenna," *Electron. Warfare*, Vol. 123, No. 6, 42–45, Jun. 2008.